AD-A064 852 DREXEL UNIV PHILADELPHIA PA DEPT OF MATERIALS ENGINEERING F/G 11/4
EFFECT OF THERMAL TREATMENT ON THE STRUCTURE AND TOUGHNESS OF T--ETC(U)
DEC 78 M H LATIF, A LAWLEY N00014-76-C-0205

UNCLASSIFIED NL

| OF |
AD
A 064 852

END
DATE
FILMED
4-79
DDC

(12) LEVEL II

AD A064852

DDC FILE COPY

Drexel University

DISTRIBUTION STATEMENT A
Approved for public release;
Distribution Unlimited

DDC
RECEIVED
FEB 23 1979
B

79 02 16 098

(12) LEVEL II

EFFECT OF THERMAL TREATMENT ON THE STRUCTURE AND TOUGHNESS OF THE Co,Cr-$(Cr,Co)_7C_3$ IN-SITU COMPOSITE

M. H. Abdel Latif and A. Lawley

December 1978

Technical Report

Office of Naval Research
Arlington, Virginia 22217

Contract N00014-76-C-0205

Drexel University
Department of Materials Engineering
Philadelphia, Pa. 19104

ABSTRACT

Work of fracture in the Co,Cr-$(Cr,Co)_7C_3$ in-situ composite has been determined at room temperature in the as-grown condition and following post-solidification isothermal exposure or thermal cycling. Toughness is low in the as-grown condition and is attributed to restricted matrix slip and a low stacking fault energy in the cobalt-rich matrix coupled with the absence of crack deflection and matrix-interface delamination. In general, the heat-treatments did not lead to any major deterioration in toughness, rather in some cases toughness was enhanced by a factor of about two over that in the as-grown composite. Changes in toughness after isothermal exposure are attributed to microstructural changes involving degeneration of the $(Cr,Co)_7C_3$ into a precipitate of $(Cr,Co)_{23}C_6$ and to fiber coarsening with an attendant increase in interfiber spacing and fiber diameter. In thermal cycling, thermal fatigue and fiber degradation are superimposed on degeneration and coarsening. A model based on thermal residual stresses and strains resulting from thermal expansion mismatch of matrix and fiber has been developed; experimental results for the two cycling regimes examined are in good agreement with the model. The increase in toughness is proportional to the temperature range of the cycle and cycles involving long times above the matrix relaxation temperature lead to creep/recovery of the matrix accompanied by a decrease in toughness.

Introduction

The high temperature stiffness and strength of several nickel and cobalt matrix in-situ composites suggest usage as a blade material in gas turbines. Apart from response to static stress, resistance to dynamic loading is important. In particular, resistance to impact damage is of major concern for structural design and there are now several in-situ eutectic alloys for which toughness data are available. Recent reviews by Lawley (1), Stoloff (2) and Jackson et al. (3) compare the various in-situ systems and assess the current level of understanding of toughness-microstructure relations.

Sources of toughness in metal-matrix composites include the matrix per se, crack deflection and/or delamination at interfaces and fiber pull-out. The high aspect ratio and interface bond integrity characteristic of many in-situ composites places a premium on the contribution of the matrix if reasonable toughness is to be realized. Other factors affecting toughness are temperature (4), fiber orientation relative to the direction of crack propagation (5,6) and fiber diameter (5,6,7).

Intrinsically, in-situ composites are stable at elevated temperatures, a characteristic derived from their solidification under near equilibrium conditions coupled with low-energy interface boundaries. However, microstructural instability with attendant property changes may occur as a result of prolonged high temperature exposure or thermal cycling. Both reflect possible in-service conditions. At a high homologous temperature, two dimensional coarsening is a factor (8) while under thermal cycling, the temperature range, cycle frequency, thermal expansion mismatch, mutual solubility and phase stability of the co-existing constituents are of primary importance (9-16).

In the present study, the room temperature toughness of the in-situ Co,Cr-$(Cr,Co)_7C_3$ composite has been evaluated in the as-grown condition and following isothermal exposure or thermal cycling treatments. The eutectic is formed by a monovariant ternary reaction and contains 30% by volume of the aligned fibrous carbide in a cobalt-rich matrix (17). The nature of the constituents suggest that the alloy might be useful as an elevated temperature structural material; the composite exhibits high strength and creep resistance and good corrosion/oxidation resistance but limited ductility (18). Preliminary work on this system has confirmed changes in toughness with thermal treatment and these have tentatively been explained in terms of the interplay of residual stress relaxation and fiber degradation (19). The work reported here has been extended to include a detailed examination and analysis of the toughness-microstructure relation in Co,Cr-$(Cr,Co)_7C_3$.

Experimental Procedure

A. Composite Preparation

Master alloy rods were prepared from 99.99% purity cobalt and chromium and spectrographic grade carbon by induction melting in an alumina crucible under argon and casting in a stainless steel mold. The overall composition of the alloy was Co-41%Cr-2.4%C by weight. Ingots 9.525 mm diameter and ∿200 mm in length were then prepared by directional solidification of the master alloy rods in closed alumina tubes under a dynamic argon atmosphere. The induction furnace was similar to that used by Thompson et al. (20) and has been described by Saatchi (21). The growth rate (R) was 7×10^{-6} m/s with a temperature gradient (G) $\sim 25 \times 10^{3}$°C/m at the liquid-solid interface of the composite. One ingot was directionally solidified at a higher growth rate (R) of 47.6×10^{-6} m/s. The corresponding G/R values at the two growth rates (35×10^{8}°C s/m^2 and 5.3×10^{8}°C s/m^2, respectively) resulted in an aligned rod-like reinforcement

of $(Cr,Co)_7C_3$ in a cobalt-rich matrix at a volume fracture $V_f = 0.3$.

B. Post-Solidification Treatments

The directionally solidified ingots were subsequently given one of four regimes of thermal treatment: (1) isothermal exposure at 913°C (T/T_m = 0.75) for times up to 26.78×10^5s; (2) isothermal exposure at 1121°C (T/T_m = 0.87) for times up to 25.9×10^5s; (3) thermal cycling between 79°C and 913°C up to 1750 cycles; (4) thermal cycling between 79°C and 1121°C up to 2500 cycles. These are shown schematically in Figure 1. The times per cycle (T_{min} to T_{max} to T_{min}) were 1250 s (60 s heating/1190 s cooling) and 1700 s (200 s heating/1500 s cooling) for thermal cycling regimes (3) and (4) respectively.

The ingots were cut into lengths of approximately 30 mm using a diamond slitting wheel. For isothermal annealing, the ingots were sealed in quartz capsules under argon. Specimens for thermal cycling were placed in a quartz tube under flowing argon and located along the focal axis of a radiant heat reflector furnace. The latter consisted of two quartz lamps with a heating zone 254 mm in length. A temperature controller and recorder were coupled to the furnace so that T_{min} and T_{max} could be preset to ±2°C.

C. Work of Fracture Determination

To determine the work of fracture, the technique and specimen configuration developed by Tattersall and Tappin (22) was used. Specimens are illustrated in Figure 2; they were precision ground to a square cross-section (6.35 mm x 6.35 mm) and cut to a length of 28.5 mm. The ligament at the center, in the shape of an isosceles triangle, was made with a 0.76 mm wide diamond slitting wheel. Specimens were loaded to failure under three-point loading in the frame of a standard Instron testing machine. In this form of test only a small load is required to initiate crack growth and the relatively slow rate of loading mitigates against energy loss due to the vibration and kinetic energy characteristic

of the standard Charpy test. A cross-head speed of 8×10^{-4} mm/s was imposed on the three-point loading fixture.

All specimens were oriented such that the carbide fiber reinforcement ran perpendicular to the plane of the triangular ligament section. The form of the load-deflection trace is shown schematically in Figure 2. Average values of the work of fracture (J/m^2) were determined as the ratio of the area under the load-deflection curve to the nominal area of the triangular ligament.

D. Metallography

Microstructures were examined optically and in the scanning electron microscope (SEM) in the as-grown condition, after each of the four heat-treatments, and following work of fracture testing. For optical metallography, specimens were wet ground through 600 grit paper, rough polished with diamond paste and given a final polish using Linde A and B aluminum oxide powder. Polished surfaces were lightly etched in aqua regia. Some specimens were also deep etched in boiling aqua regia to partially remove the matrix and reveal carbide morphology by SEM. Fracture surfaces were also examined directly by SEM.

Experimental Results and Observations

A. Microstructures

Representative optical micrographs of the composite in the as-grown condition are illustrated in Figure 3; transverse and longitudinal sections are included for both growth rates employed. SEM provides a three-dimensional characterization of the carbide-fiber morphology, Figures 3(e) and 3(f). Consistent with previous observations on this composite (17), the aligned fibrous carbide reinforcement is highly irregular in terms of cross-sectional dimensions and geometry. Carbide branching is evident and the aspect ratio varies over a wide range. Faceting of fiber cross-sections is evident in Figures 3(a), 3(c), 3(e) and 3(f). This reflects the hexagonal symmetry of the

carbide fibers (17). The interfiber spacing (λ) was determined statistically and found to vary about a mean of 3.53μm for a growth rate of 7×10^{-3}mm.s^{-1}. At the higher growth rate of 47.6×10^{-3}mm.s^{-1}, $\bar{\lambda}$ was 1.5μm.

The effect of isothermal exposure and thermal cycling on the microstructure of Co,Cr-$(Cr,Co)_7C_3$ is considered for each of the four post-heat treatments in turn:

(1) During isothermal exposure at 913°C, small fiber branches develop on the main carbide fibers and grow out into the matrix. These have been observed after 25.9×10^4s. The number of branches increases with time and subsequently these break up into discrete precipitates, approximately spherical in shape which coarsen on further exposure. Degradation of the main fibers,in terms of gross non-uniformity in diameter, is seen after 26.78×10^5s. This sequence of changes in composite microstructure is illustrated in Figures 4 and 5. Energy dispersive analysis (21) confirms that the precipitates are $(Cr,Co)_{23}C_6$, consistent with previous work by Thompson et al. (17) on this composite system and observations by Lane and Grant (23) on the stability of Cr_7C_3. Thus, at 913°C the composite consists of $(Cr,Co)_{23}C_6$ precipitates and $(Cr,Co)_7C_3$ fibers in a cobalt rich matrix.

(2) There is no evidence for branching, precipitation or fiber degradation at 1121°C for times up to 25.92×10^5s. However, microstructural instability is reflected in a coarsening of the $(Cr,Co)_7C_3$ carbide reinforcement with an associated decrease in rod density (# of rods per unit area). The effect is more pronounced in composites grown at the higher rate (47.6×10^{-3} mm/s) since fiber diameter and inter-fiber spacing in the as-grown condition are smaller than for the lower growth rate (7×10^{-3} mm/s). Representative fiber morphologies

are illustrated in Figure 6 and the change in rod density (N) with time for each growth rate in Figure 7. Values of N were calculated from the interfiber spacing (λ) by assuming a hexagonal carbide distribution in the matrix in which case:

$$N = \frac{2}{\sqrt{3}} \cdot \lambda^{-2} \qquad (1)$$

Values of λ and N and the standard deviation of each are summarized in Table I.

(3) and (4) Fiber braching, similar to that occurring at 913°C, is observed for both thermal cycling regimes. There is no accompanying fiber degradation up to 1792 cycles between 79°C and 913°C. In contrast, thermal cycling between 93°C and 1121°C does promote fiber degradation. Changes in fiber morphology for the two regimes of thermal cycling are shown in Figures 8 and 9. Since fiber branching did not develop at 1121°C, the composite must spend sufficient time in the vicinity of 913°C (during each heating/cooling cycle between 79°C and 1121°C) to allow branching and fiber degeneration to occur.

B. Work of Fracture

In the as-grown condition, the average work of fracture at room temperature is 14.7 KJ/m^2, with peak loads $\sim$2670N. These are in good agreement with values reported by Thompson (6) for this composite using a similar test-piece configuration and fiber orientation.

Most of the load-deflection traces approximated the profile shown schematically on the left hand side of Figure 2. Thus, fracture begins when the load reaches P_{ℓ_1}, after which the load drop to zero is almost instantaneous, corresponding to catastrophic crack growth. A few specimens

gave load-deflection traces with a small 'tail', as shown schematically on the right hand side of Figure 2. The extent of the tail was in the range 5-10% of the total area under the load-displacement curve; this corresponds to a component of slower or more-controlled crack growth in the final stages of fracture.

The dependence of work of fracture and peak load on isothermal exposure at 913°C and 1121°C is shown in Figures 10 and 11 respectively. While considerable scatter exists, particularly following exposure at 913°C, it is concluded that toughness is not impaired for times up to 25×10^6s. On the contrary, the data suggest an improvement in work of fracture relative to that of the as-grown material. The composites exposed at 913°C experience an increase in G_f and P_ℓ which peak after $\sim 15 \times 10^5$s. At 1121°C, G_f and P_ℓ increase with exposure times up $\sim 10 \times 10^5$s, after which both parameters stay relatively constant at a level above that of the as-grown material, Figure 11. A similar response is noted for both growth speeds examined.

The work of fracture of the composite after thermal cycling between 79°C and 913°C is shown in Figure 12, and between 79°C and 1121°C in Figure 13. For both regimes there is a significant increase in both G_f and P_ℓ up to a maximum at about 500 cycles; this is followed by a decrease in the two parameters for higher numbers of cycles. Figure 12 shows that after 1742 cycles (79°C - 913°C), G_f and P_ℓ exceed the levels of the as-grown material. Over the 79°C - 1121°C range, G_f after 2500 cycles (10.9 kJ/m^2) is lower than that in the as-grown condition (14.7 kJ/m^2), Figure 13.

Load-deflection traces following isothermal exposure or thermal cycling typically showed a rapid load drop to zero from P_ℓ. In the few specimens exhibiting a 'tail', the contribution to the total area under the load-deflection curve was small ($\sim$5-10%) i.e. similar to that noted in the as-grown condition. No significant or systematic differences could be established between

the extent of the 'tail' and the associated post-solidification heat-treatment.

C. Fracture Morphology

On a macroscopic scale, the fracture surfaces from test pieces displaying an abrupt load drop from P_ℓ (i.e. no tail) were relatively flat. This was true in the as-grown material and for each of the four heat-treatments. A typical fracture surface profile for an as-grown composite is shown in Figure 17(a). The fracture surface profile characteristic of the few specimens exhibiting a 'tail' on the load-deflection trace is seen in Figure 17(b).

Representative micrographs (SEM) of the flat fracture surfaces are illustrated in Figure 18. Fibers always fail by cleavage and the matrix shears locally to link up the fiber breaks, Figure 18(a). There was no evicence of delamination at matrix-fiber interfaces or of fiber pull-out. Occasionally, splitting of the fibers in the longitudinal direction was observed, Figure 18(b).

Discussion

A. Work of Fracture - As-Grown Condition

The form of the load-deflection traces and the associated flat fracture surfaces reflect low inherent toughness in the Co,Cr-$(Cr,Co)_7C_3$ in-situ composite at ambient temperatures. Jackson et al. (3) have compared the room temperature impact energies of several nickel and cobalt-base aligned eutectics and that of René 80. The comparison is given in Table II along with the work of fracture data from the present study. Tattersall and Tappin (22) have shown that for a given material, the Charpy V-notch test gives an impact energy about one order of magnitude higher than that determined by the work

of fracture method. This is due to the energy expended on vibration and in imparting kinetic energy to the fractured pieces in the Charpy test. Even allowing for this effect it is clear that the toughness of the Co,Cr-$(Cr,Co)_7C_3$ composite is lower than that of the other in-situ composites listed in Table II.

In a parallel study (24) of the fatigue crack response of Co,Cr-$(Cr,Co)_7C_3$ at room temperature, it has been shown that fracture toughness is low, and inferior to that of rod-like CoTaC and lamellar γ/γ'-δ or γ-δ. The low fracture toughness was rationalized in terms of three contributing factors, and each will also contribute to a low work of fracture:

(1) The cobalt-rich matrix is expected to have a low stacking fault energy. In consequence dislocations are confined to their slip planes, giving rise to planar slip and to stress concentrations which lead to matrix cracking along these planes. These conditions are conducive to fiber shearing, as observed in this study.

(2) At room temperature, the cobalt-rich matrix has a hexagonal close-packed structure with a limited number of operative slip systems. This coupled with a low stacking fault energy promotes stress concentration at the crack tip.

(3) The interfacial matrix-carbide bond in the Co,Cr-$(Cr,Co)_7C_3$ composite is strong. This is confirmed by a lack of fiber pull-out or interface delamination in this and a previous impact study (19) and under static (21) and fatigue (24) loading. In contrast, crack deflection and delmaination occur in lamellar γ/γ'-δ (25), and interface delamination and deformation twinning of the δ phase in lamellar γ-δ with subsequent twin boundary fracture (26). Each of the above mechanisms is absent in Co,Cr-$(Cr,Co)_7C_3$ and therefore cannot contribute to toughness.

The absence of an effect of growth rate (and hence fiber diameter) on work of fracture in the as-grown condition is evident from Figure 11 and is at variance with Thompson's results on this composite (6). While no explanation is offered, it should be noted that in the latter study the difference in work of fracture with fiber diameter was small: 15.1 kJ/m^2 at 3.9μm diameter and 13.5 kJ/m^2 at 1.4μm diameter. Also, the fiber diameters in the present study were smaller (2.03μm and 0.86μm) than those in Thompson's material.

B. Work of Fracture - Effect of Heat-Treatment

(a) Isothermal Exposure

Isothermal exposure at 913°C results in the development of branches of $(Cr,Co)_{23}C_6$ on the main $(Cr,Co)_7C_3$ fibers and the branches subsequently break up into discrete precipitates, Figure 4. Saatchi (21) has shown that this change in the microstructure of the composite is accompanied by an increase in strength as a result of the dispersion hardening effect of the incoherent precipitates in the cobalt-rich matrix. In the context of the work of fracture test, this is manifest as an increase in peak load P_ℓ and hence in a larger area under the load-displacement curve.

It is also possible that the precipitates of $(Cr,Co)_{23}C_6$ act to locally deflect the crack, thereby increasing toughness. The recent observations by Scarlin (27) on creep crack propagation in this composite are pertinent. Thus, the $(Cr,Co)_{23}C_6$ precipitate develops in bands (rings) around the remaining $(Cr,Co)_7C_3$ fibers and the creep crack is deflected at, and propagates for short distances along, the bands (i.e., parallel to the direction of reinforcement) before continuing in a direction perpendicular to the applied stress.

The subsequent decreases in G_f and P_ℓ after exposure times $\geq 15 \times 10^5$s are possibly due to the coarsening of the $(Cr,Co)_{23}C_6$ precipitates - with an accompanying decrease in strength, and hence peak load. Relaxation of matrix stresses, either by matrix recovery or creep may also be a contributing factor to the decrease in work of fracture following long-time exposure at 913°C.

Isothermal exposure at 1121°C does not lead to precipitation of $(Cr,Co)_{23}C_6$. However, microstructural change is reflected in a coarsening of the rod-like $(Co,Cr)_7C_3$ reinforcement, Figure 7. It is therefore reasonable to associate the observed increase in work of fracture (Figure 11) with the increase in fiber diameter and/or interfiber spacing. Cooper and Kelly (28) have proposed a model for crack propagation in composites which predicts a linear dependence of work of fracture on fiber diameter. With the simplifying assumption that the carbide rods are cylindrical and are distributed uniformly in the matrix in a hexagonal array:

$$V_f = \frac{\sqrt{3}\pi}{6} \frac{d^2}{\lambda^2} = \frac{N\pi d^2}{4} \qquad (2)$$

where d is the fiber diameter. Using equation (2) with $V_f = 0.3$, the fiber diameters corresponding to the experimentally determined values of λ (Table I) in the as-grown condition (i.e., $\lambda = 3.53\mu m$ for $R = 7 \times 10^{-6}$m/s; $\lambda = 1.5\mu m$ for $R = 47.6 \times 10^{-6}$m/s) are 2.03μm and 0.86μm, respectively. After exposure at 1121°C for 25.92×10^5s, the corresponding fiber diameters (equation (2)) are 4.23μm and 2.18μm.

There is an inconsistency in the data in Figure 11 in that for all exposure times, the composite grown at the lower rate (7×10^{-3}mm/s) possessed larger diameter fibers than the composite grown at 47.6×10^{-3}mm/s. However, the latter material exhibited the higher work of fracture for a given time of exposure at 1121°C. An explanation for this is not readily apparent.

(b) Thermal Cycling

Both thermal cycling regimes give rise to an initial increase in G_f and P_ℓ with a peak in each at ∿500 cycles, Figures 12 and 13. This variation of the work of fracture can be understood in terms of thermal residual stresses and microstructural change accompanying thermal cycling.

If the thermal expansion coefficients (α) of the two constituents in a composite are not equal, axial internal stresses will develop on thermal cycling. The elastic stresses are proportional to the product of the expansion mismatch $\Delta\alpha$ and the temperature interval ΔT. In Co,Cr-$(Cr,Co)_7C_3$, α(matrix) is larger than α(carbide) and the residual stresses are compressive in the carbide and tensile in the matrix.

For elastic strains, and as an approximation for small plastic strains, the axial residual stresses in the matrix (σ_m) and fiber (σ_f) are given by (9, 29):

$$\sigma_m = \int_{T_1}^{T_2} \frac{(E_m E_f V_f \Delta\alpha)dT}{(E_f V_f + E_m V_m)} \qquad (3)$$

$$\sigma_f = \int_{T_1}^{T_2} \frac{(E_m E_f V_m \Delta\alpha)dT}{(E_f V_f + E_m V_m)} \qquad (4)$$

where E, V and α are Young's modulus, volume fraction and thermal expansion coefficient respectively, T_1 and T_2 are the temperature limits of the integration, m and f refer to the matrix and fiber reinforcement respectively. Similarly, the axial residual strains associated with $\Delta\alpha$ are given by:

$$\varepsilon_m = \int_{T_1}^{T_2} \frac{(E_f V_f \Delta\alpha)dT}{(E_f V_f + E_m V_m)} \qquad (5)$$

$$\varepsilon_f = \int_{T_1}^{T_2} \frac{(E_m V_m \Delta\alpha)\, dT}{(E_f V_f + E_m V_m)} \qquad (6)$$

From the literature, the temperature dependence of E_m, E_f, α_m and α_f can be calculated (Appendix I). These parameters (as a function of T) were substituted into equations (3) through (6) with $V_f = 0.301$. An exact solution was developed for the above integrals and a computer program used to calculate σ_m, σ_f, ε_m, and ε_f as a function of temperature. The temperature limits are $T_1 = 293°K$ and T_2 = the relaxation temperature above which residual stresses are relaxed by matrix creep, i.e., $\alpha_m = \alpha_f$. $T_2 \simeq 1033°K$ for the Co,Cr-$(Cr,Co)_7C_3$ in-situ composite (4,30).

Results of the computations are given in Figure 14. T_1 and T_2 are the same for both thermal cycling regimes; in consequence, the matrix and fiber stresses and strains are identical for either regime at a given temperature between T_1 and T_2. In combination, Figures 1 and 14 give the residual matrix strains as a function of time in both thermal cycling regimes. These are shown in Figure 15.

It is proposed that the strain cycling occurring in the composite leads to fatigue hardening with an accompanying increase in strength. The increase in P_ℓ gives a higher work of fracture G_f since the area under the load-deflection curve is increased. According to the model, the temperature dependence of the matrix strain is the same for both thermal cycling ranges so that the magnitude/increase in G_f should be identical in each. Comparison of Figures 12 and 13 show this to be the case. G_f reaches a peak value $\sim$28 kJ/m^2 after 530 cycles for cycling regime III and after 540 cycles for cycling regime IV.

This model can also account for the subsequent decrease in G_f as a result of matrix creep or recovery. The time spent by the composite above the relaxation temperature during each cycle may be thought of as an "apparent hold time", i.e., the time available for relaxation of the matrix by creep or recovery. From

Figure 15, the apparent hold times are 64s and 207s for cycling regimes III and IV respectively. It is therefore predicted that the decrease in G_f beyond the peak should be sharper and larger for regime IV than for regime III. This is seen to be the case, cf. Figures 12 and 13.

The longer time at higher temperatures in regime IV should enhance fiber degradation. Evidence for this is provided in Figures 8 and 9. While no fiber degradation was observed under regime III for up to 1742 cycles, some degradation was evident under regime IV after 1143 cycles and considerable degradation after 2505 cycles.

The effect of other cycling regimes on work of fracture in this composite provides further support for the model. Lin et al. (19) imposed cycles with a fixed maximum temperature (1121°C) but with minimum temperatures of 80°C, 400°C and 538°C. Data was reported in terms of the normalized work of fracture D_f, defined as the ratio of G_f after thermal cycling to G_f in the as-grown composite. D_f is shown as a function of number of cycles in Figure 16.

In the model, thermal residual stresses and strains are proportional to the ΔT of the cycle. Since the maximum temperature was 1121°C in each regime, the residual stresses and strains, and their effect on D_f, should be higher for the lower minimum temperature. The data in Figure 16 show this to be the case.

Also included in Figure 16 are D_f values for cycling between 400°C and 1121°C with a hold time of 3600 s at 1121°C. The small peak in G_f followed by a significant drop in G_f is consistent with the concept of matrix creep on recovery plus fiber degradation taking place during the holding period at 1121°C.

The implications of structural change on toughness are now considered. The effects of the degeneration of $(Cr,Co)_7C_3$ (i.e., branching) and of fiber degradation will be superimposed on the thermal residual stress mechanism.

While both cycling regimes III and IV give rise to the degeneration reaction (Figures 8 and 9), fiber degradation is restricted to cycling regime IV. Fiber branching and formation of the $(Cr,Co)_{23}C_6$ precipitate cause an increase in strength but fiber degradation lowers composite strength. Thus these factors work in opposition in their effect on the work of fracture but to an unknown extent.

In a number of monocarbide-reinforced in-situ composites, the carbide has been shown to develop surface serrations during thermal cycling (14-16). These can result in either an increase or decrease in strength depending on the alloy and cycling conditions. No evidence for surface serrations on the carbide was found in the Co,Cr-$(Cr,Co)_7C_3$ in-situ composite as a result of thermal cycling.

Conclusions

1. Isothermal exposure at 913°C leads to an increase in the room temperature levels of G_f and P_ℓ (compared to the as-grown condition) up to a peak at $\sim 15 \times 10^5$s, beyond which both parameters decrease. These changes are attributed to a degeneration reaction of the $(Cr,Co)_7C_3$ carbide. Microstructurally, fibers branch and a fine-scale precipitate of $(Cr,Co)_{23}C_6$ develops, followed by coarsening.

2. Isothermal exposure at 1121°C leads to an increase in the room temperature levels of G_f and P_ℓ (compared to the as-grown condition); the increase in both parameters is sustained for exposure times up to 25.92×10^5s. The changes in G_f and P_ℓ are the result of fiber coarsening with attendant increases in interfiber spacing and fiber diameter. Degeneration of the $(Cr,Co)_7C_3$ does not occur at 1121°C.

3. Both thermal cycling regimes III and IV give rise to a sharp increase in G_f and P_ℓ after ∿500 cycles beyond which both parameters decrease. These changes are associated with the degeneration reaction and thermal fatigue. Fiber degradation, manifest in non-uniformity of the carbide diameter, is a further factor affecting G_f and P_ℓ in regime IV.

4. A model based on thermal residual stresses and strains resulting from the thermal expansion mismatch of matrix and fiber has been developed. Experimental results for both thermal cycling regimes III and IV are in good agreement with the model. Increases in G_f and P_ℓ are due to thermal residual strains in the matrix which are proportional to ΔT in the thermal cycle. The longer the composite spends above the matrix relaxation temperature in each cycle, the more extensive is matrix creep and/or recovery and fiber degradation. In combination, these are responsible for the subsequent decrease in G_f and P_ℓ beyond ∿500 cycles.

5. In general, the four post-solidification heat-treatments did not lead to a major deterioration in toughness compared to the as-grown condition.

6. The toughness of the Co,Cr-$(Cr,Co)_7C_3$ is low in comparison to other in-situ composites and is attributed to the low stacking fault energy of the matrix, a restricted number of slip systems and to the absence of crack deflection or interface delamination. Cracks propagate readily through both matrix and fibers.

References

1. A. Lawley, Conference on In-Situ Composites-II, Edited by M. R. Jackson, J. L. Walter, F. D. Lemkey and R. W. Hertzberg, Xerox Individualized Publishing, Lexington, Mass., p. 451, 1976.

2. N. S. Stoloff, in Advances in Composite Materials, Edited by G. Piatti, Applied Science Publishers Ltd., London, p. 274, 1978.

3. M. R. Jackson, J. L. Walter and M. F. Henry, "Evaluation of DS Eutectic Superalloys for Turbine Blade Applications", Quarterly Report #4, Contract #NAS3-19711, General Electric Res. and Dev. Center, 1976.

4. P. R. Sahm and T. Varga, Proc. Conference on In-Situ Composites, National Materials Advisory Board, Report #NMAB 308-II, National Academy of Sciences - National Academy of Engineering, Washington, D.C., p. 239, 1973.

5. M. J. Salkind and F. D. George, Trans. Met. Soc. AIME, 1968, Vol. 242, p. 1237.

6. E. R. Thompson, J. Composite Materials, Vol. 5, p. 235, 1971.

7. A. S. Yue and B. T. Kaba, in Composite Reliability, ASTM STP #580, American Society for Testing and Materials, Phila., Pa., p. 504, 1975.

8. H. B. Smartt and T. H. Courtney, Met. Trans., 7A, 123, 1976.

9. E. M. Breinan, E. R. Thompson and F. D. Lemkey, Proceedings of the Conference on In-Situ Composites, National Materials Advisory Board, National Academy of Sciences, 1973, #308-I, p. 201.

10. M. Gell, Specialists Meeting on Directionally Solidified In-Situ Composites, Editors: E. R. Thompson and P. R. Sahm, AGARD Conf. Proc. #156, Technical Editing and Reproduction Ltd., London, 1974, p. 117.

11. D. A. Woodford, J. Materials Science and Engineering, 1976, Vol. 24, p. 257.

12. H. R. Gray and W. A. Sanders, Conference on In-Situ Composites-II, Editors: M. R. Jackson, J. L. Walter, F. D. Lemkey and R. W. Hertzberg, Xerox Press, Lexington, Mass., 1976, p. 201.

13. D. A. Woodford, ibid., p. 211.

14. F. M. Dunlevy and J. F. Wallace, Met. Trans. A, 1974, Vol. 5A, p. 1351.

15. F. H. Harf and S. N. Tewari, Met. Trans. A, 1977, Vol. 8A, p. 202.

16. D. A. Woodford, Met. Trans. A, 1977, Vol. 8A, p. 2016.

17. E. R. Thompson and F. D. Lemkey, Met. Trans., 1970, Vol. 1, p. 2799.

18. E. R. Thompson, D. A. Koss and J. C. Chesnutt, Met. Trans., 1970, Vol. 1, p. 2807.

19. L. Y. Lin, M. H. AbdelLatif and A. Lawley, Proc. Second Int. Conference on Composite Materials, The Metallurgical Society of AIME Editors: R. Noton, R. Signorelli, K. Street and L. Phillips, 1978, p. 770.

20. E. R. Thompson, F. D. George and E. M. Breinan, Proceedings Conf. on In-Situ Composites, National Materials Advisory Board, National Academy of Sciences, 1973; #308, p. 71.

21. H. Saatchi, "Microstructural Stability and Strength of the Monovariant Co,Cr-$(Cr,Co)_7C_3$ Composite", June 1978 Ph.D. Thesis, Drexel University, Philadelphia, Pa.

22. H. G. Tattersall and G. Tappin, Journal of Materials Science, 1966, Vol. 1, p. 296.

23. J. R. Lane and N. J. Grant, Trans. ASM, 1952, Vol. 44, p. 113.

24. M. H. AbdelLatif and A. Lawley, "Fatigue Crack Propagation in a Co,Cr-$(Cr,Co)_7C_3$ Composite". Submitted to Met. Trans., 1979.

25. A. Yuen and G. R. Leverant, Met. Trans. A, 1976, Vol. 7A, p. 1443.

26. W. R. Hoover and R. W. Hertzberg, Met. Trans. A, 1971, Vol. 2A, p. 1283 and p. 1289.

27. R. B. Scarlin, Met. Trans., A, 1977, Vol. 8A, p. 1941.

28. G. A. Cooper and A. Kelly, J. Mech. Phys. Solids, 1967, 15, #4, p. 279.

29. C. A. Hoffman, "Effects of Thermal Loading on Composites with Constituents of Differing Thermal Expansion", NASA Tech. Note NASA-TDN-D-5926, August 1970.

30. D. A. Koss and S. M. Copley, Met. Trans., 1971, Vol. 2, p. 1557.

31. International Critical Tables of Numerical Physics, Chemistry and Technology; Editor: E. W. Washburn, McGraw Hill, 1927, Vol. 2, p. 465.

Table I

Effect of Isothermal Exposure at 1121°C on Carbide Spacing and Density in Co,Cr-$(Cr,Co)_7C_3$

(a) Growth rate 7×10^{-6} m/s

Time (5×10^5)	0(as-grown)	3.46	7.78	18.04	25.92
$\bar{\lambda}$(μm)	3.53	3.99	5.73	6.78	7.4
Standard Deviation	±2.4	±1.75	±2.3	±2.84	±3.9
$N(\mu m)^{-2}$	0.092	0.072	0.035	0.025	0.021
Standard Deviation	±0.02	±0.018	±0.014	±0.012	±0.011

(b) Growth rate 47.6×10^{-6} m/s

Time (5×10^5)	0(as-grown)	3.46	7.78	18.04	25.92
$\bar{\lambda}$(μm)	1.5	1.65	2.0	2.72	3.79
Standard Deviation	±0.8	±1.0	±1.2	±1.3	±2.1
$N(\mu m)^{-2}$	0.518	0.42	0.29	0.155	0.08
Standard Deviation	±0.08	±0.07	±0.06	±0.055	±0.03

Table II

Impact Energies of In-Situ Composites

Material	Condition	Mini Charpy*	Standard Charpy*	Work of Fracture Specimen	Reference
γ'/γ-Mo	As-grown	1560	-	-	3
Ni-10Cr-TaC	As-grown	460	-	-	3
Co-15Cr-TaC	As-grown	170	250	-	3
Co-15.7Cr-0.5Ni-3W-TaC	As-grown	230	310	-	3
Ni-TaC	As-grown	370	660	-	3
Co,Cr-$(Cr,Co)_7C_3$	As-grown	-	-	14.7	This study
Co,Cr-$(Cr,Co)_7C_3$	15×10^5s at 913°C	-	-	28	This study
Co,Cr-$(Cr,Co)_7C_3$	25×10^5s at 1121°C	-	-	20	This study
Co,Cr-$(Cr,Co)_7C_3$	500 cycles (79°C-913°C)	-	-	28	This study
Co,Cr-$(Cr,Co)_7C_3$	500 cycles (79°C-1121°C)	-	-	29	This study
René 80	Cast	-	80	-	3

* V-notch energies

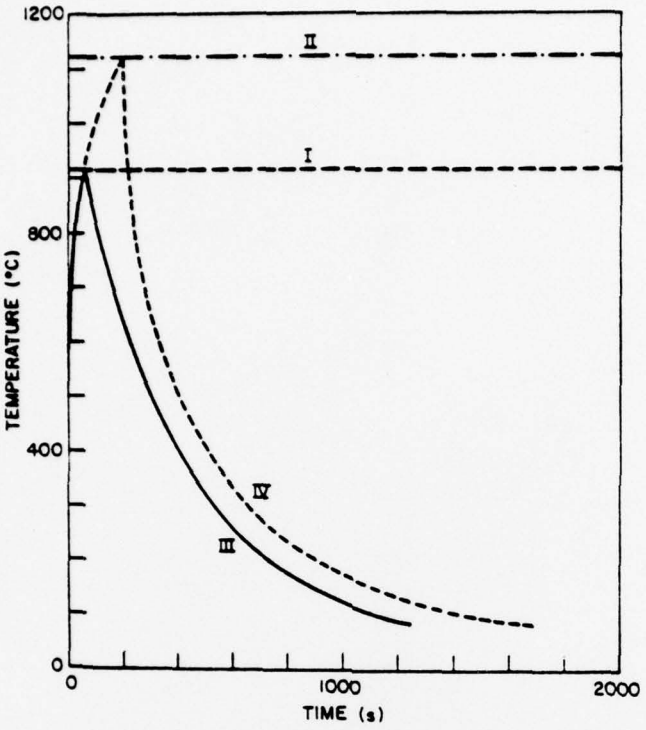

Figure 1. The isothermal (I and II) and thermal cycling (III and IV) treatments.

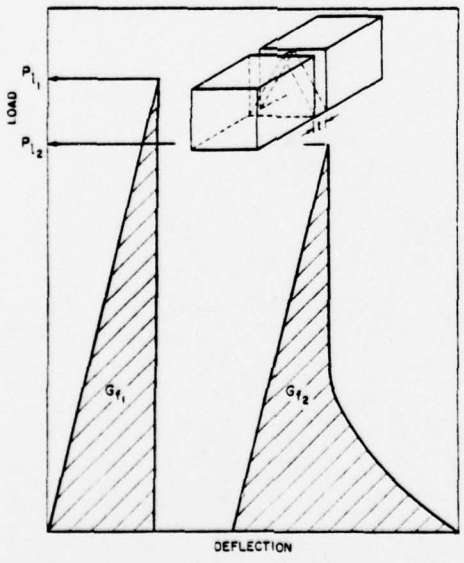

Figure 2. Specimen for determination of work of fracture and load-deflection trace (schematic). t = 0.76 mm.

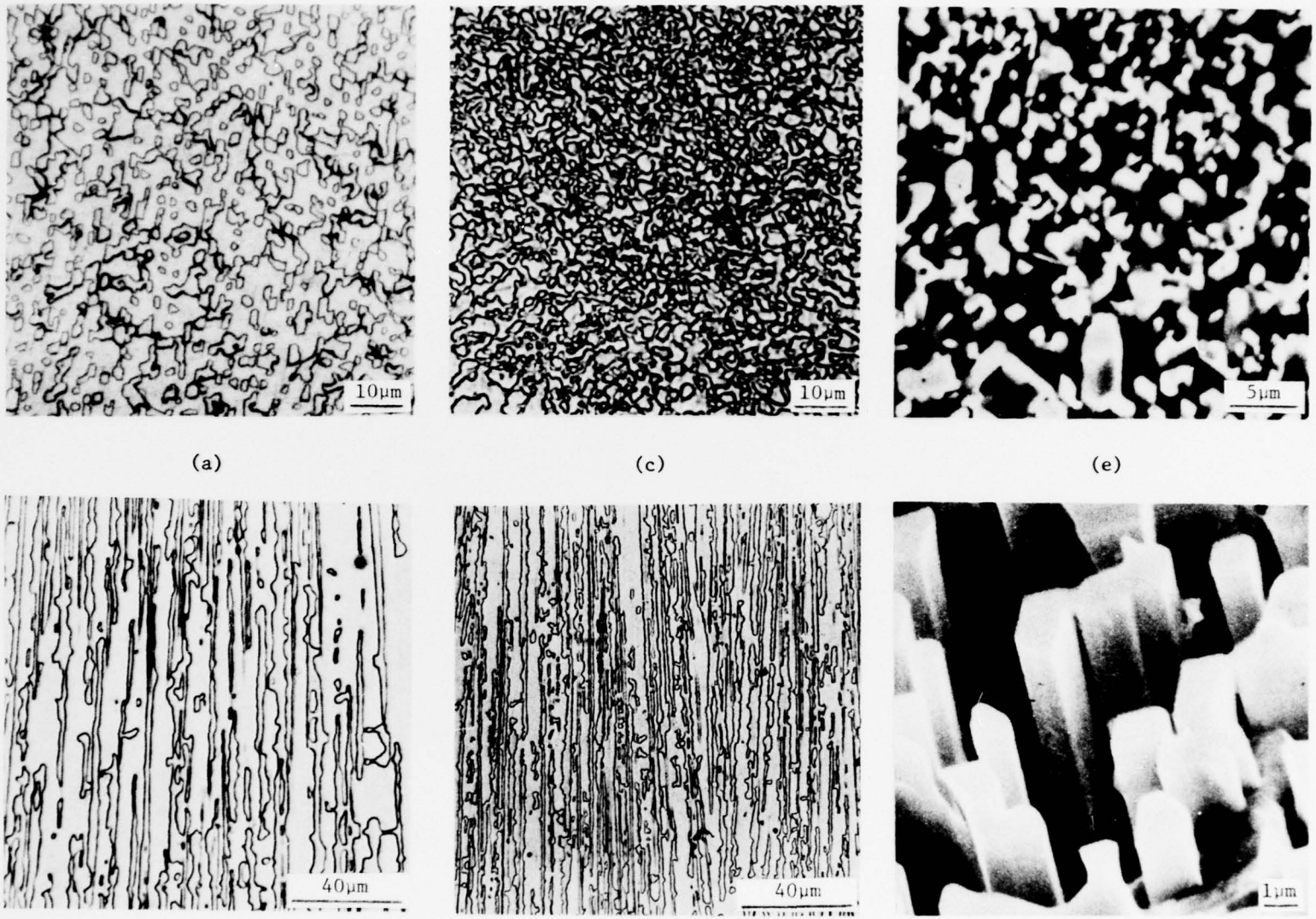

Figure 3. Transverse (a,c) and longitudinal (b,d) section optical micrographs and SEM (e,f). As-grown condition. Growth rate 7 x 10^{-6} m/s in a, b, e, and f; 47.6 x 10^{-6} m/s in c and d.

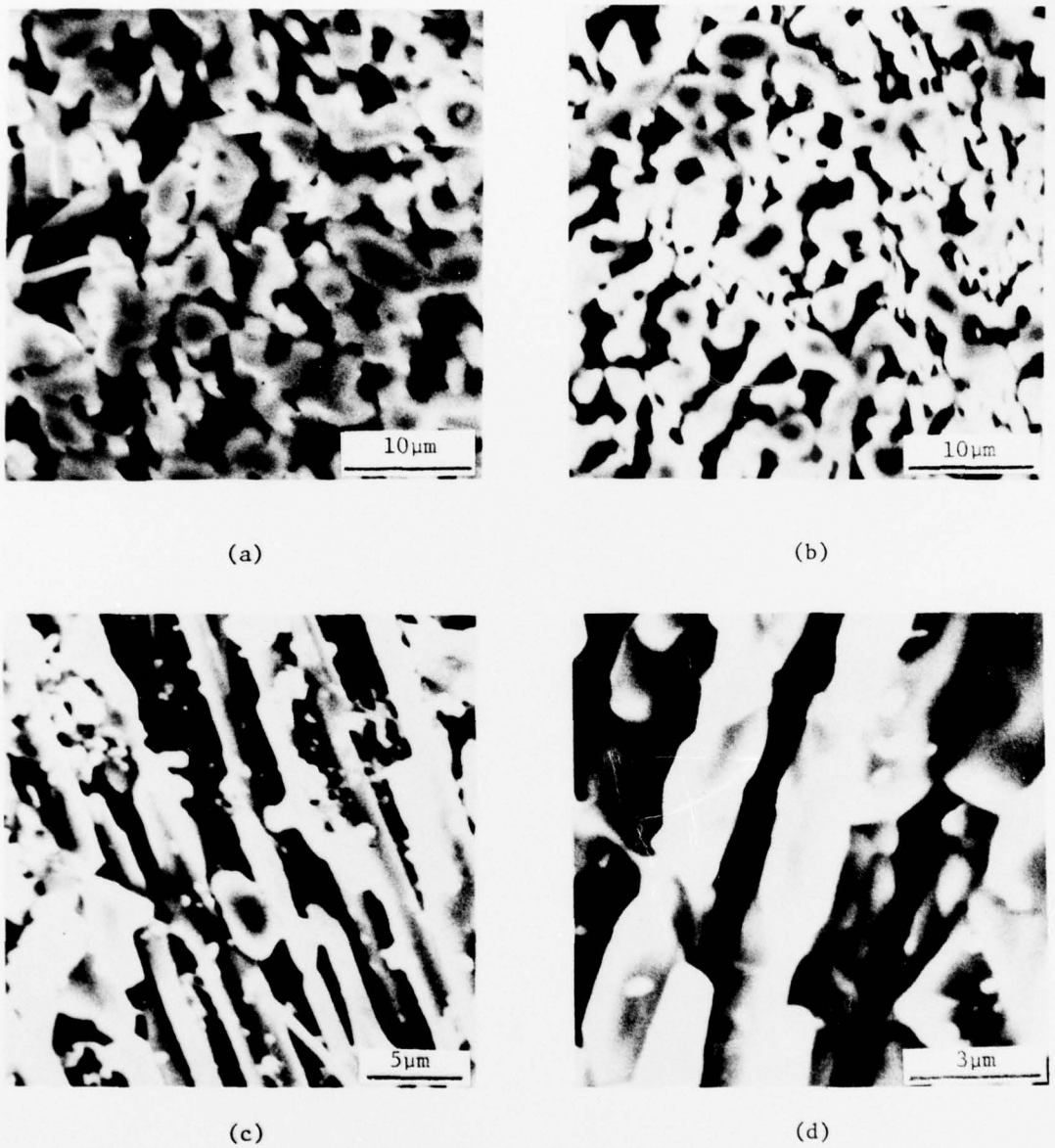

(a) (b)

(c) (d)

Figure 4. SEM after exposure at 913°C; growth rate 7 x 10^{-6}m/s. (a) 25.92 x 10^{4}s; (b) 10.37 x 10^{5}s; (c) 19 x 10^{5}s; (d) 26.78 x 10^{5}s.

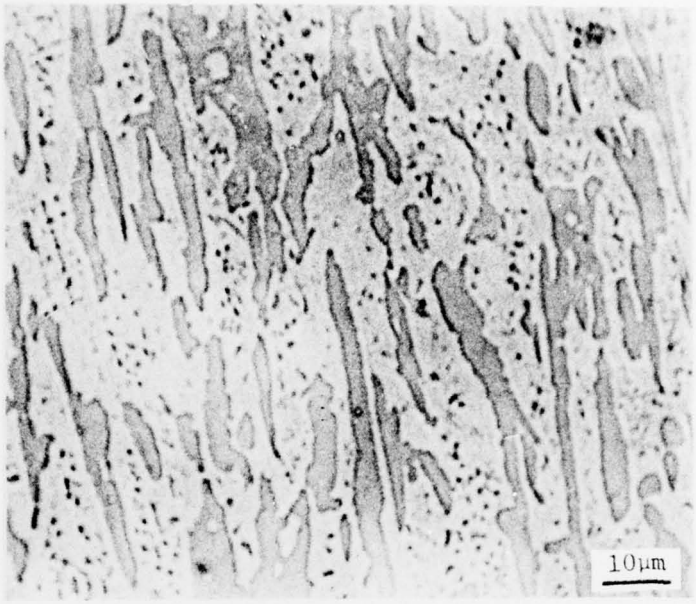

Figure 5. Longitudinal section optical micrograph after 26.78×10^5s at 913°C; growth rate 7×10^{-6} m/s.

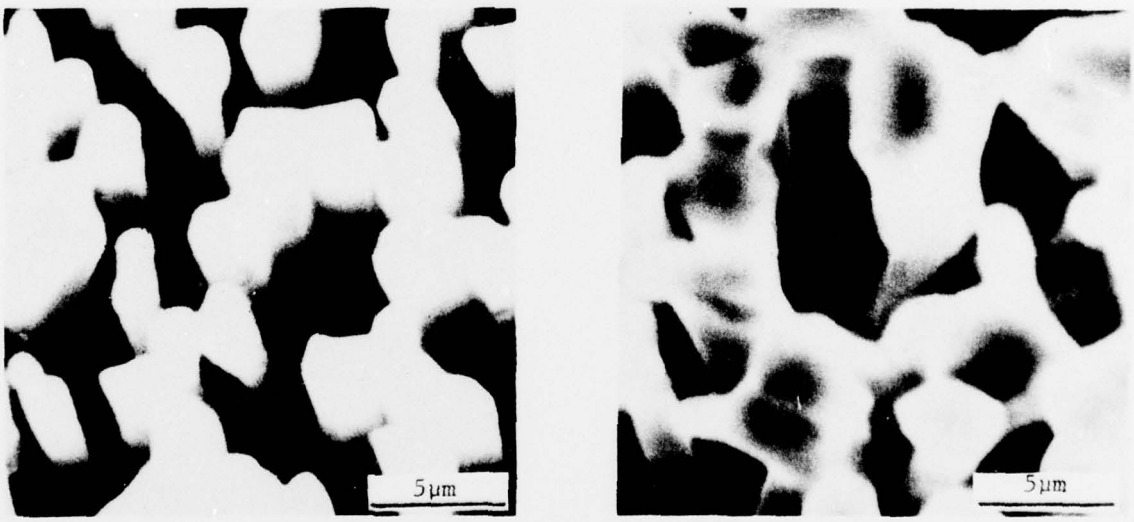

(a) (b)

Figure 6. SEM after exposure at 1121°C; growth rate 7×10^{-6}m/s. (a) 3.45×10^5s; (b) 25.92×10^5s.

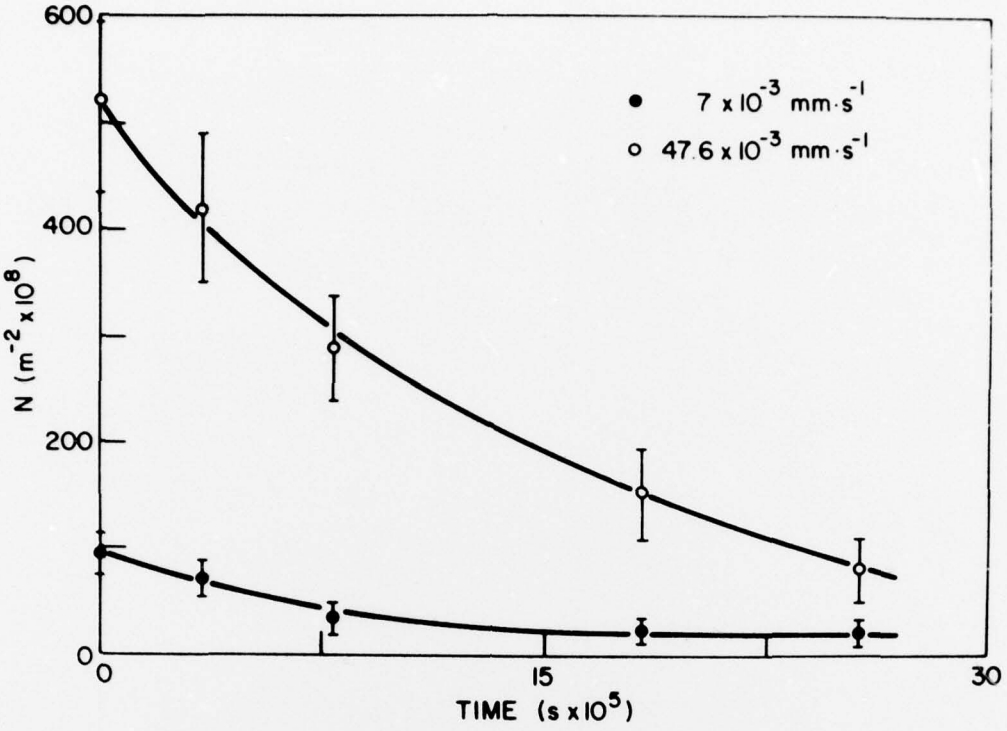

Figure 7. Fiber density (N) as a function of time at 1121°C for composites solidified at different growth rates.

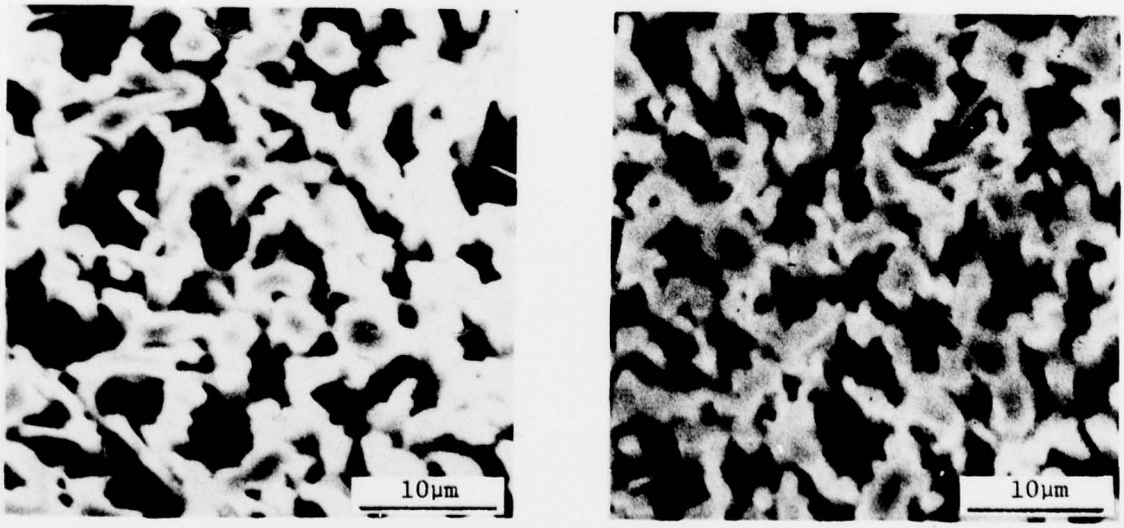

(a) (b)

Figure 8. SEM after thermal cycling between 79°C and 913°C. (a) 807 cycles; (b) 994 cycles; growth rate 7×10^{-6} m/s.

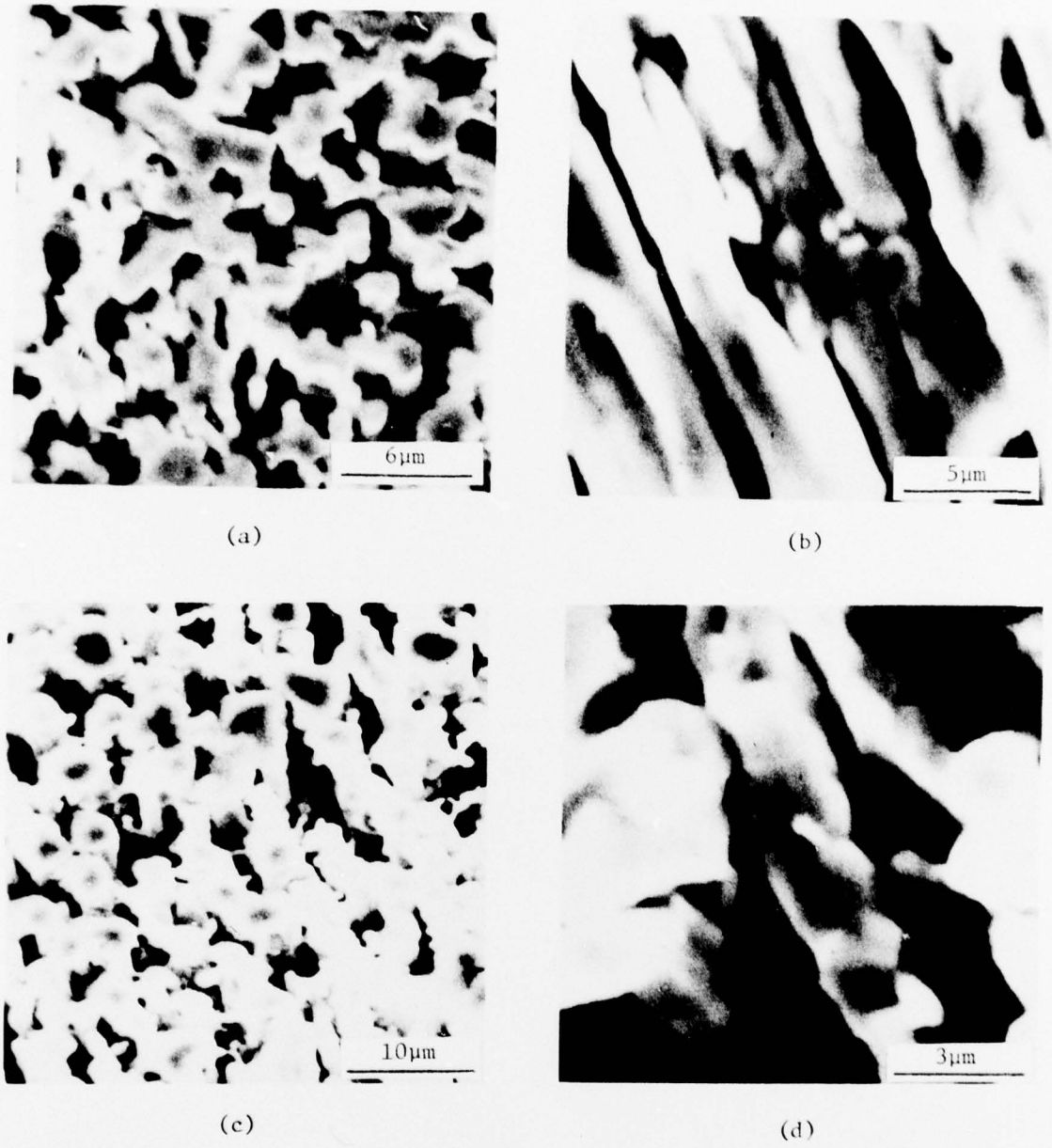

Figure 9. SEM after thermal cycling between 79°C and 1121°C. (a) 400 cycles; (b) 1143 cycles; (c) 2505 cycles; (d) 2505 cycles; growth rate 7 x 10^{-6} m/s.

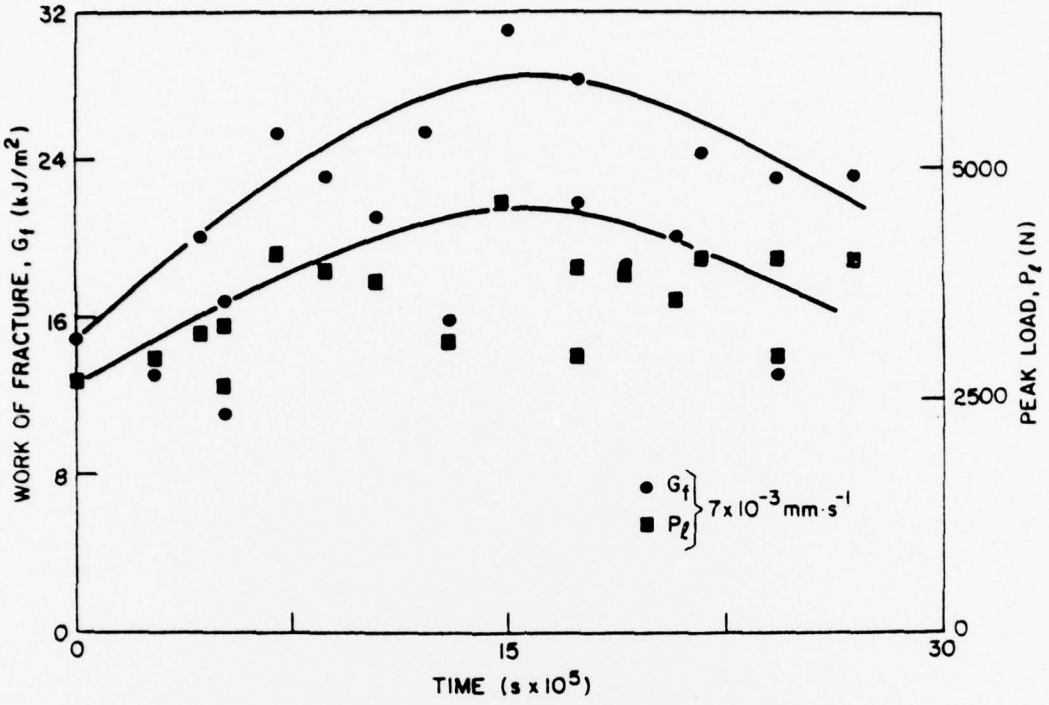

Figure 10. Work of fracture (G_f) and peak load (P_ℓ) after isothermal exposure at 913°C.

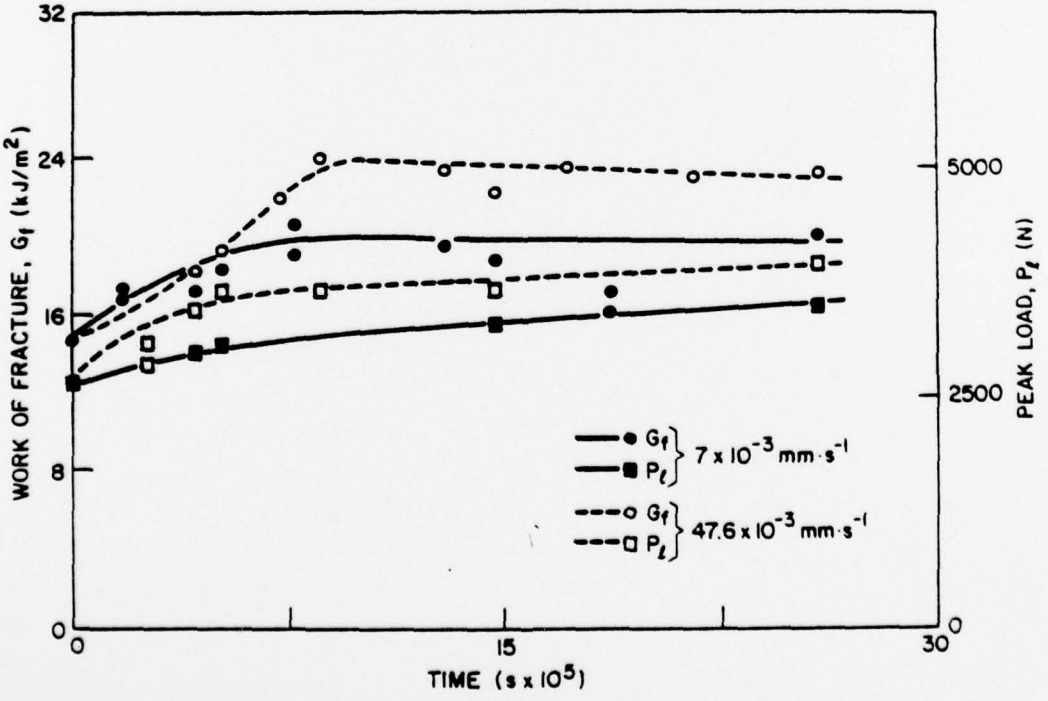

Figure 11. Work of fracture (G_f) and peak load (P_ℓ) after isothermal exposure at 1121°C.

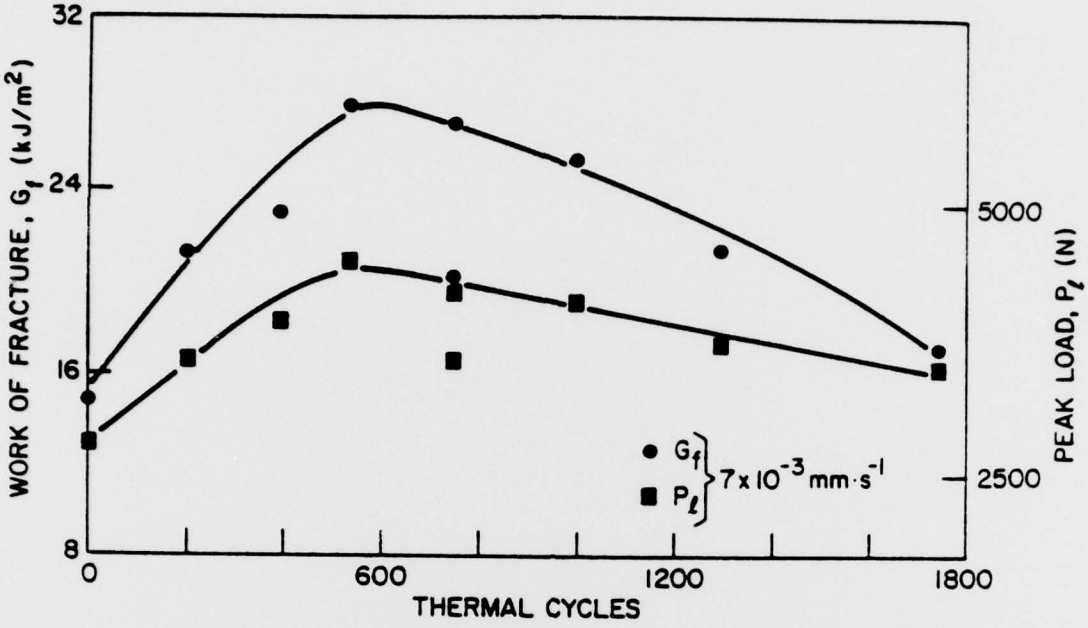

Figure 12. Work of fracture (G_f) and peak load (P_ℓ) after thermal cycling between 79°C and 913°C.

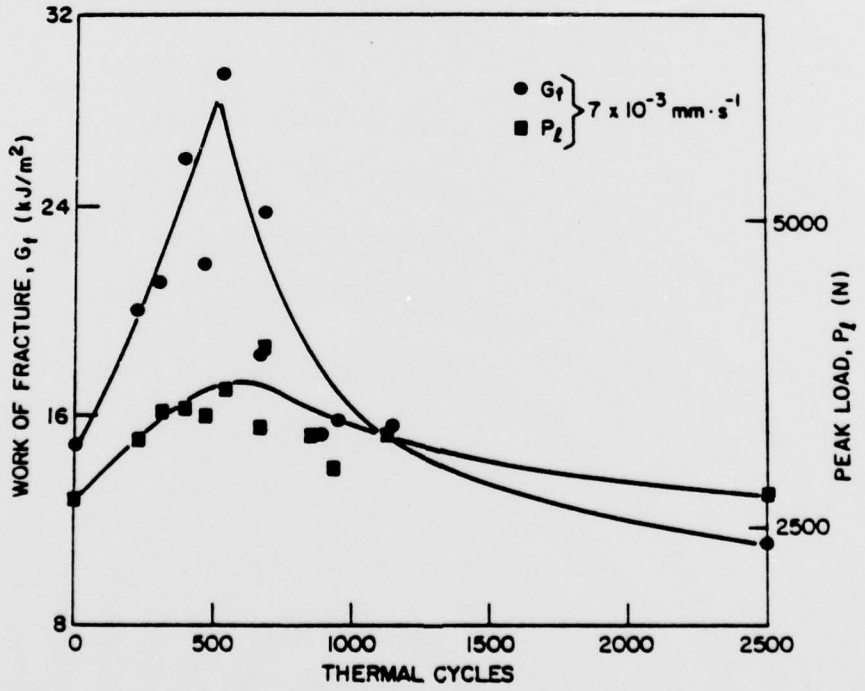

Figure 13. Work of fracture (G_f) and peak load (P_ℓ) after thermal cycling between 79°C and 1121°C.

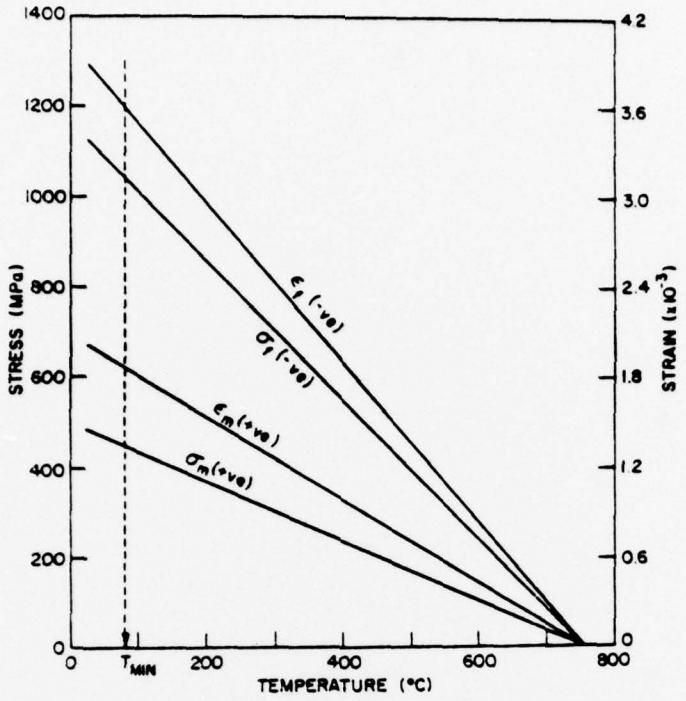

Figure 14. Calculated thermal stresses and strains in matrix and fiber as a function of temperature.

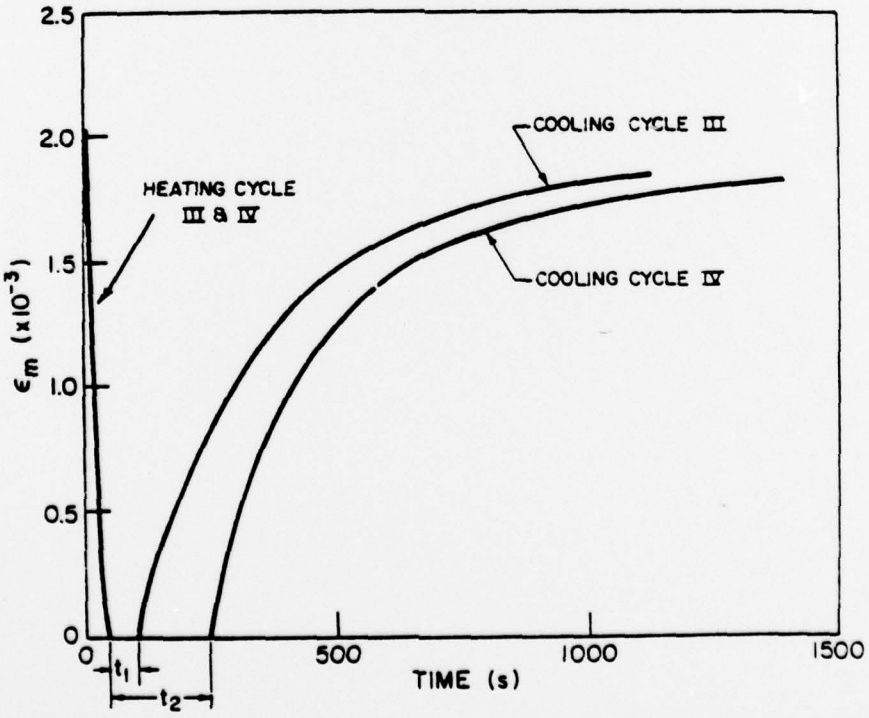

Figure 15. Thermal strains in the matrix as a function of the two thermal cycling treatments.

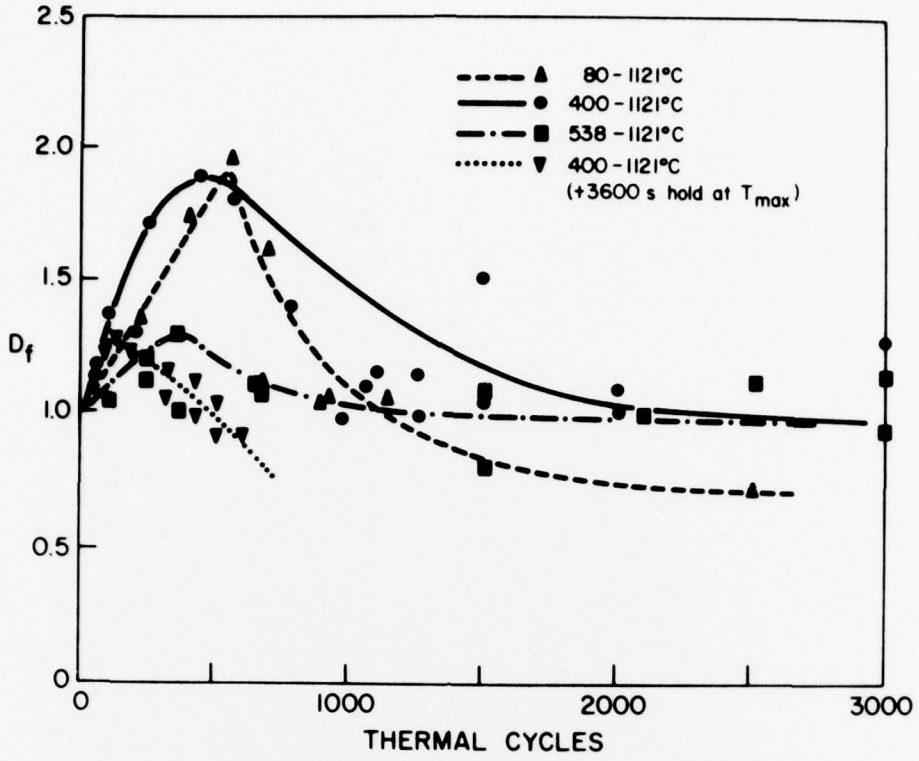

Figure 16. The normalized work of fracture D_f after thermal cycling as a function of cycling regime.

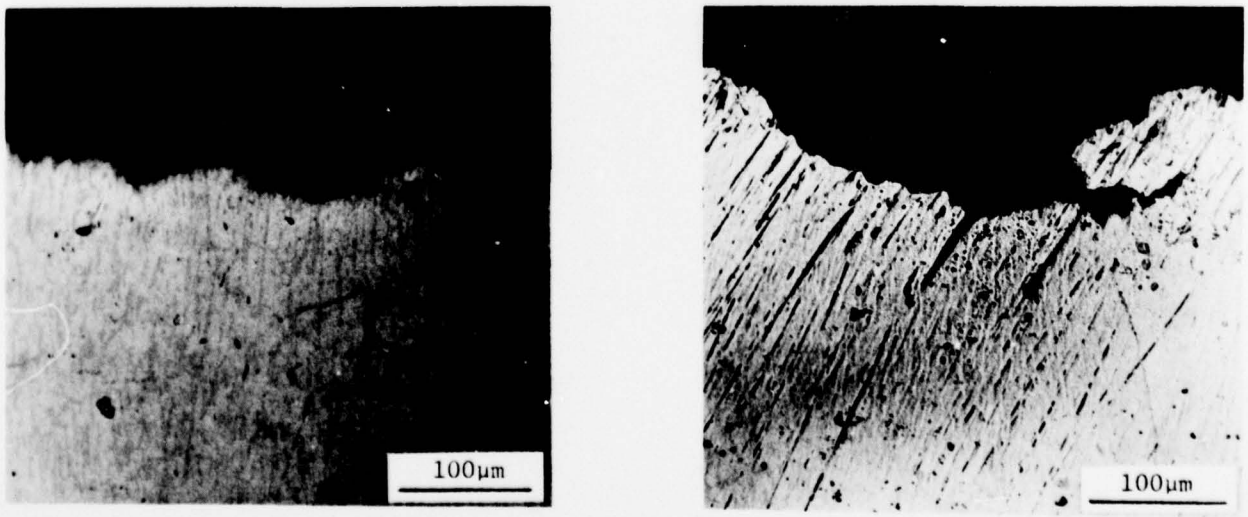

(a) (b)

Figure 17. Optical micrographs showing fracture surface profile. (a) abrupt load drop from P_ℓ, (b) load drop with tail - see Figure 2.

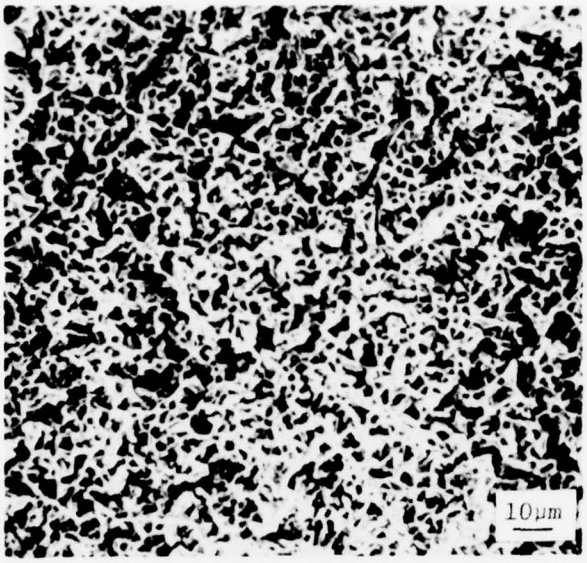

(a)

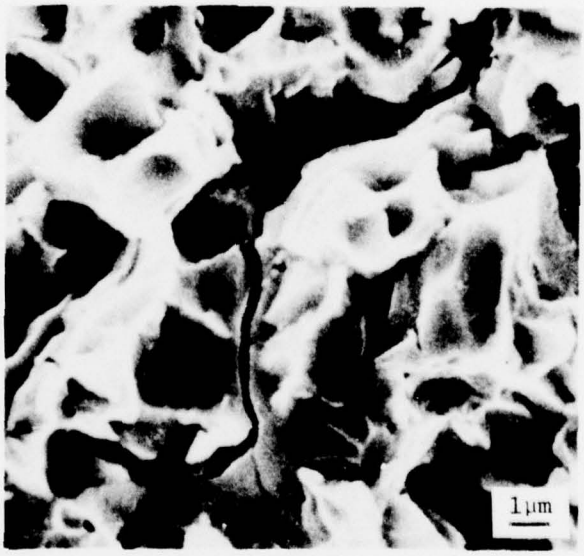

(b)

Figure 18. SEM of fracture surfaces after 431 cycles between 400°C and 1121°C.

Appendix I

Temperature Dependence of Young's Modulus and Coefficient of Thermal Expansion

The elastic moduli of the Co,Cr-$(Cr,Co)_7C_3$ composite and the matrix alone decrease linearly with temperature (18) according to the relations:

$$E_c = 276.94 - 0.0745T \qquad \text{(A-1)}$$

$$E_m = 260.62 - 0.0894T \qquad \text{(A-2)}$$

where E_c and E_m are in GPa and T is in °K.

From the rule of mixtures:

$$E_f = \frac{E_c - E_m V_m}{V_f} \qquad \text{(A-3)}$$

Substituting from equations (A-1) and (A-2) in (A-3), and with $V_f = 0.301$:

$$E_f = 314.86 - 0.04T \qquad \text{(A-4)}$$

Similarly, the thermal expnasion coefficients of matrix and carbide increase linearly with temperature and follow the relations (31):

$$\alpha_f = 10 + 0.001T \qquad \text{(A-5)}$$

$$\alpha_m = 15 + 0.005T \qquad \text{(A-6)}$$

where α_f and α_m are in units of $10^{-6}\,°K^{-1}$. Room temperature values of α_f and α_m are taken from reference (30).

Unclassified

SECURITY CLASSIFICATION OF THIS PAGE (When Data Entered)

REPORT DOCUMENTATION PAGE		READ INSTRUCTIONS BEFORE COMPLETING FORM
1. REPORT NUMBER	2. GOVT ACCESSION NO.	3. RECIPIENT'S CATALOG NUMBER
4. TITLE (and Subtitle) Effect of Thermal Treatment on the Structure and Toughness of the Co,Cr-$(Cr,Co)_7C_3$ In-Situ Composite		5. TYPE OF REPORT & PERIOD COVERED Technical Report December 1978 6. PERFORMING ORG. REPORT NUMBER
7. AUTHOR(s) M. H. Abdel Latif and A. Lawley		8. CONTRACT OR GRANT NUMBER(s) N00014-76-C-0205
9. PERFORMING ORGANIZATION NAME AND ADDRESS Department of Materials Engineering Drexel University Philadelphia, Pa. 19104		10. PROGRAM ELEMENT, PROJECT, TASK AREA & WORK UNIT NUMBERS
11. CONTROLLING OFFICE NAME AND ADDRESS Office of Naval Research Arlington, Va. 22217		12. REPORT DATE December 1978 13. NUMBER OF PAGES 35
14. MONITORING AGENCY NAME & ADDRESS(if different from Controlling Office)		15. SECURITY CLASS. (of this report) Unclassified 15a. DECLASSIFICATION/DOWNGRADING SCHEDULE
16. DISTRIBUTION STATEMENT (of this Report) Unlimited DISTRIBUTION STATEMENT A Approved for public release; Distribution Unlimited		
17. DISTRIBUTION STATEMENT (of the abstract entered in Block 20, if different from Report)		
18. SUPPLEMENTARY NOTES		
19. KEY WORDS (Continue on reverse side if necessary and identify by block number) In-situ composite, cobalt-rich matrix, carbide reinforcement, isothermal exposure, thermal cycling, microstructure, fractography, strength, work of fracture.		

20. ABSTRACT (Continue on reverse side if necessary and identify by block number)
Work of fracture in the Co,Cr-$(Cr,Co)_7C_3$ in-situ composite has been determined at room temperature in the as-grown condition and following post-solidification isothermal exposure or thermal cycling. Toughness is low in the as-grown condition and is attributed to restricted matrix slip and a low stacking fault energy in the cobalt-rich matrix coupled with the absence of crack deflection and matrix-interface delamination. In general, the heat-treatments did not lead to any major deterioration in toughness, rather in some cases toughness

DD FORM 1 JAN 73 1473 EDITION OF 1 NOV 65 IS OBSOLETE
S/N 0102-014-6601

Unclassified

SECURITY CLASSIFICATION OF THIS PAGE (When Data Entered)

20. Continued

was enhanced by a factor of about two over that in the as-grown composite. Changes in toughness after isothermal exposure are attributed to microstructural changes involving degeneration of the $(Cr,Co)_7C_3$ into a precipitate of $(Cr,Co)_{23}C_6$ and to fiber coarsening with an attendant increase in interfiber spacing and fiber diameter. In thermal cycling, thermal fatigue and fiber degradation are superimposed on degeneration and coarsening. A model based on thermal residual stresses and strains resulting from thermal expansion mismatch of matrix and fiber has been developed; experimental results for the two cycling regimes examined are in good agreement with the model. The increase in toughness is proportional to the temperature range of the cycle and cycles involving long times above the matrix relaxation temperature lead to creep/recovery of the matrix accompanied by a decrease in toughness.